Monatshefte für Chemie - Chemical Monthly (2020) 151:549–557
https://doi.org/10.1007/s00706-020-02571-z

ORIGINAL PAPER

Efficient synthesis, characterization, and in vitro bactericidal studies of unsymmetrically substituted triazole-derived Schiff base ligand and its transition metal complexes

Sajjad H. Sumrra[1] · Ifza Sahrish[1] · Muhammad A. Raza[1] · Zahoor Ahmad[3] · Muhammad N. Zafar[2] · Zahid H. Chohan[4] · Muhammad Khalid[5] · Saeed Ahmed[5]

Received: 22 November 2019 / Accepted: 25 February 2020 / Published online: 31 March 2020

Abstract

In the present research, novel unsymmetrically substituted triazole-derived Schiff base ligand 2-[[[5-[[1-(5-methylfuran-2-yl)-ethylidene]amino]-1*H*-1,2,4-triazol-3-yl]imino]methyl]phenol (L) has been synthesized by the reaction of 1,2,4-triazole-3,5-diamine with 2-hydroxybenzaldehyde and with 5-methyl-2-acetylfuran in an equimolar ratio. The synthesized ligand L was characterized by physical methods (melting point, solubility, color) as well as by spectral techniques (IR, UV–Vis, ^{1}H NMR, ^{13}C NMR, and MS), elemental analysis, and computational studies. Computational analysis further elucidated the structure, polarity, stability, and nature of the ligand. The bivalent(II), trivalent(III), and tetravalent(IV) transition metal complexes were formed by reacting Mn(II), Fe(II), Co(II), Ni(II), Cu(II), Zn(II), and Cr(III) metals as chloride and, VO(IV) as sulfate with Schiff base ligand L in 1:2 (M:L) molar ratio. Ligand was coordinated with the metal ions, VO via benzaldehyde-O and azomethine-N and with Mn(II), Fe(II), Co(II), Ni(II), Cu(II), Zn(II), and Cr(III) via benzaldehyde-O, azomethine-N, and triazole-N. The structure of the metal complexes was deduced by IR, conductance, magnetic moments, and elemental analysis. Biological evaluation of triazole-derived Schiff base ligand and its metal complexes was carried out against bacterial strains, *Escherichia coli*, *Staphylococcus aureus*, *Neisseria gonorrhea*, and *Pseudomonas syringae*. Copper complex showed the highest inhibition against all bacterial strains as compared to the free ligand and amongst other metal complexes. In vitro antibacterial studies thus concluded that the prepared ligand showed bioactivity which was enhanced upon chelation/coordination with the metal ions.

Graphic abstract

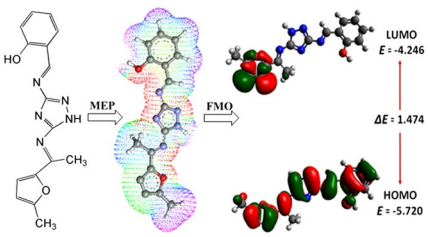

Keywords 1,2,4-Triazole Schiff base · Unsymmetrical ligand · Transition metal chelates · FMOs · MEP · Antibacterial activity

Introduction

Metal-based antimicrobial compounds are effectively used because of resistance of microbes [1]. Metal-based antimicrobial agents have therefore, emerged as a promising and

Electronic supplementary material The online version of this article (https://doi.org/10.1007/s00706-020-02571-z) contains supplementary material, which is available to authorized users.

Extended author information available on the last page of the article

potential area of research in metal-based drug chemistry [2]. Heterocyclic compounds having various heteroatoms such as O, N, or S have a tendency of forming coordination compounds/metal chelates used as active antimicrobial agents [3]. 1,2,4-Triazole is one of the most significant aromatic heterocyclic nitrogen-rich compounds. Many biological active triazole-based compounds such as itraconazole, albaconazole, fluconazole, posaconazole, isavuconazole, voriconazole, ravuconazole, ketoconazole [4, 5] and others are well-known antibacterial [6], antiviral [7], antifungal [8, 9], anti-inflammatory [10], anticonvulsant [11], antiproliferative [12], anticancer [13], and antitubercular agents[14]. These triazole compounds also show remarkable biological applications as enzyme inhibitors, i.e., urease and lipase inhibitors [15] because of low toxicity, good pharmacodynamic and pharmacokinetic profiles [16, 17]. Various potential substitutions in triazole molecule are chemically possible to changes its bioactive chemistry into more potentially used drugs [18, 19]. Triazole also forms spiro-heterocyclic and Schiff base compounds by reacting with other biologically active molecules resulting in more active compounds [20, 21]. These compounds have more than one site to coordinate with the metal atoms [22] to form more stable bioactive triazole-based transition metal complexes [23]. Different studies have shown that when the bioactive compounds are coordinated with the metal atoms their bioactivity is enhanced [24]. Keeping this in consideration, previously, we have synthesized symmetrically substituted biologically active metal-based triazoles and in this paper we wish to report unsymmetrically substituted novel metal-based triazoles. These compounds have been evaluated for their antibacterial activity against selected Gram-positive and Gram-negative bacterial species such as *Escherichia coli*, *Staphylococcus aureus*, *Neisseria gonorrhea*, and *Pseudomonas syringae*. Copper complex overall showed the highest inhibition against all bacterial strains as compared to the free ligand and amongst other metal complexes.

Results and discussion

Chemistry

Unsymetrically substituted triazole-derived Schiff base ligand 2-[[[5-[[1-(5-methylfuran-2-yl)ethylidene]-amino]-1*H*-1,2,4-triazol-3-yl]imino]methyl]phenol (**L**) was prepared by the condensation reaction of 1,2,4-triazole-3,5-diamine with 2-hydroxybenzaldehyde (step 1) with 5-methyl-2-acetylfuran (step 2) in an equimolar ratio under reflux as shown in Scheme 1. The synthesized Schiff base ligand was soluble in hot ethanol, dioxane, DMF, and DMSO. The composition of the ligand was consistent with their microanalytical and spectral data. The metal complexes **1**–**8** were obtained by the reaction of the corresponding ligand with the metal ions Co(II), Ni(II), Cu(II), Zn(II), Cr-(II), Mn (II), Fe (II), and VO(II) as chlorides and vanadium as sulfate in a 1:2 (metal:ligand) molar ratio. All the metal complexes were air and moisture stable at room temperature. They were insoluble in common organic solvents and only soluble in ethanol, DMF, and DMSO. The triazole ligand and its metal complexes were formed using solvent (ethanol). All the compounds were obtained in specific color with good yield ranging from 71 to 80%. Melting point provided a strong clue about formation of ligand and its metal complexes. Physical measurements and analytical data of the complexes **1**–**8** are given in Table S1 (Scheme 2).

^{1}H NMR spectral studies

The ligand showed characteristic peaks in proton NMR spectra and supported formation of ligand. The appearance of singlet peak at $\delta = 9.14$ ppm represented the presence of azomethine proton C^{7}-*H*. The proton C^{9}-*H* of triazole moiety showed singlet peak at 14.28 ppm. The protons of aromatic ring such as C^{5}-*H*, C^{2}-*H*, C^{3}-*H*, and C^{4}-*H* showed peaks at 7.85, 7.67, 7.49, and 7.40 ppm as doublet as well as triplet. The furan protons C^{13}-*H* and C^{14}-*H* of ligand E-3 displayed peaks at 7.00 and 6.95 ppm as doublet. The

Scheme 1

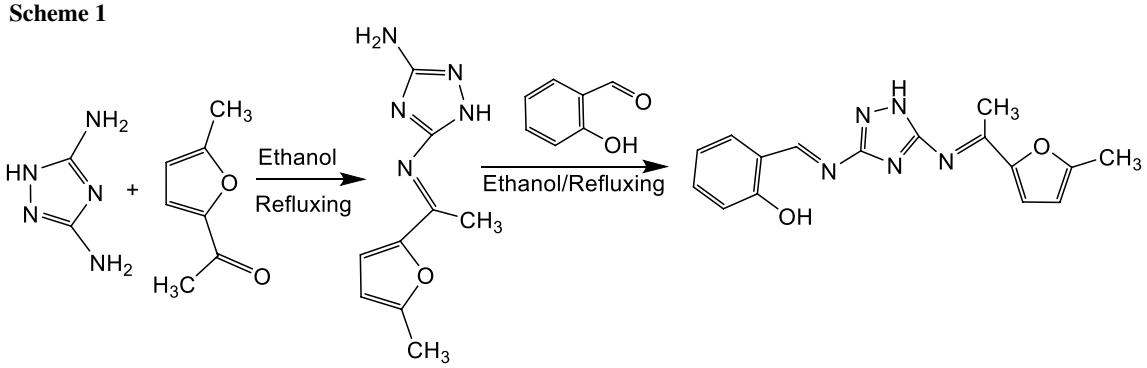

Scheme 2

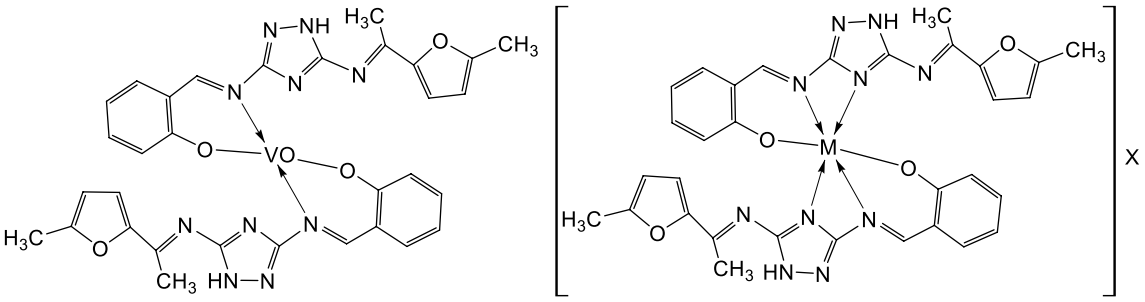

1

2; X = Cl **3-8**; X = 0

M = Cr, Mn, Fe, Co, Ni, Cu, Zn

peaks of methyl protons C^{16}-*H* and C^{11}-*H* observed at 2.49 and 3.32 ppm. In proton NMR spectra of ligand, another singlet peak was found at 12.79 ppm due to C^{1}-*H*. In proton NMR spectra, peaks of NH_2 and carbonyl protons were not found which revealed the condensation reaction occurred. The value of all protons of ligand was found to be in its expected region.

^{13}C NMR spectral studies

The ^{13}C NMR spectral studies gave a strong clue about formation of ligand. The ^{13}C NMR spectra showed characteristics peaks within range. In NMR spectra, the azomethine (C=N) carbons C^{10} and C^{7} peaks appeared at $\delta = 163.07$ and 161.68 ppm and supported strongly the condensation reaction that occurred within ligand. The triazole carbon C^{6} showed peak at 160.19 ppm. The aromatic ring of ligand showed chemical shifts at 119.08, 132.44, 119.27, 133.39, and 116.559 ppm due to C^{6}, C^{5}, C^{4}, C^{3}, and C^{2} protons. The peaks at 13.56 and 13.70 ppm represented carbons C^{16} and C^{11} of methyl groups of ligand. The peak of carbon C^{1} attached to hydroxyl group was observed at 156.68 ppm.

Mass spectral studies of ligand

Mass spectral studies of ligand strongly supported the formation of triazole-based ligand. The fragment of molecular ion was found to be as $[C_{16}H_{14}N_5O_2]^+$. The peak of ligand formed at $m/z = 308$ was due to loss of a proton and considered as molecular ion peak. Proposed mass fragmentation pattern of the ligand followed the cleavage of C–C, C–N, C–O exocylic and endocyclic bonds. The base peak (100% intensity) of ligand appeared at $m/z = 290.1$ with most stable fragment $[C_{16}H_{12}N_5O]^+$. In the mass spectra of ligand, various peaks were appeared with specific intensity and fragments were produced with specific mass-to-charge ratio [25].

UV–Vis spectral studies

UV–Vis spectra of triazole-based ligand and its complexes showed various types of bands. The appearance of bands represented different kinds of transitions in compounds, supported synthesis of ligand as well as coordination between metal ions and ligand. The UV–Vis spectra of all compounds (solutions were prepared in DMSO) were recorded at room temperature and scanned in the range between 200 and 800 nm wavelengths. The ligand showed two absorption bands due to π–π^* and n-π^* transitions. A broadband appeared at 297 nm and 420 nm due to π–π^* and n-π^* transitions [26]. The appearance of first band gave an idea about the presence of aromatic benzene ring, while the appearance of second band provided information about the presence of azomethine (HC=N) group within the synthesized ligand. In case of metal complexes, coordination between ligand and metal ions was easily analyzed. The second band due to n-π^* transition was shifted to longer wavelength indicated the transfer of electron from ligand to metals. In case of metal complexes, the appearance of other band was due to d–d transitions [27].

Computational studies

The optimized geometric parameters of ligand are tabulated in Tables S2 and S3 (Supplementary Information). They are compared with reported experimentally determined parameters [28, 29]. The comparative analysis showed that the calculated geometric parameters are in good agreement with reported bond lengths which are determined by DFT-based calculations and experimental technique (Fig. 1).

Frontier molecular orbitals (FMOs)

FMOs such as LUMO and HOMO play an important role to understand the chemical stability of synthesized compound. Four significant molecular orbital pairs as

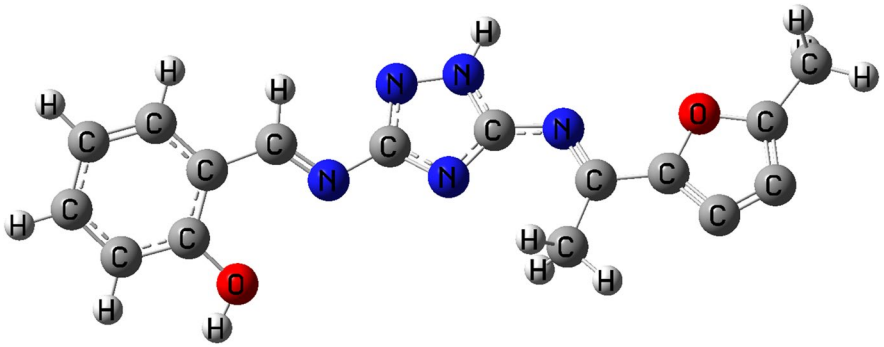

Fig. 1 Optimized structure of triazole ligand **L**

HOMO → LUMO, HOMO-1 → LUMO + 1, HOMO-2 → LUMO + 2, and HOMO-3 → LUMO + 3 have been investigated by means of M06-2X/6-311G (d, p) level. Energy gap between HOMO → LUMO, HOMO-1 → LUMO + 1, HOMO-2 → LUMO + 2, and HOMO-3 → LUMO + 3 is observed to be 1.47, 4.20, 5.09, and 6.78 eV, respectively. It is considered that the energy gap is inversely related to reactivity and directly associated with the stability of the molecule. With the help of HOMO and LUMO energies, global reactivity descriptors were calculated with the assistance of following equations.

Global reactivity descriptors have been determined using below equations:

$$IP = -E_{\mathrm{HOMO}} \tag{1}$$

$$EA = -E_{\mathrm{LUMO}} \tag{2}$$

where *IP* is the ionization potential/a.u, *EA* is the electron affinity/a.u. Koopmans's theorem [30] has been used to determine the chemical hardness (η) which is defined as:

$$\eta = \frac{[IP - EA]}{2} = -\frac{\left[E_{LUMO} - E_{HOMO}\right]}{2} \tag{3}$$

Global softness (σ) is defined by the following relationship [31]:

$$\sigma = \frac{1}{2\eta} \tag{4}$$

The *IP* value (6.883 eV) of title molecule is found to be greater than the value of *EA* (1.561 eV) which denotes the greater electron donating capability as compared to acceptor potential of title molecule. Chemical hardness (η) value 1.47 eV is also noticed to be very large as compared to its softness (σ) value of 0.68 eV. Greater *IP* value than *EA* and larger hardness value than softness imply that the investigated molecule is hard and kinetically stable molecule with donor characteristics useful in charge transfer reactions which might be reason of said ligand to form the complexes (Fig. 2).

Molecular electrostatic potential (MEP)

Molecular electrical potential map helped in understanding distribution of charges in ligand and also known as electrostatic potential energy maps or molecular electrical potential surfaces. The reactive site of a compound can also be predicted sing MEP method. The MEP allowed visualizing the charged regions of a ligand. The diagram contained three colors red, blue, and white which distinguish different types of atoms in the ligand. The electronegative region within ligand was represented by red color, while electropositive region was represented by blue color. A light color such as white described the non-polar region of ligand. The positive and negative regions displayed attraction for electrophilic and nucleophilic attacks [32] (Fig. 3).

Mulliken atomic charges of ligand

The Mulliken population analysis played a role in the utilization of quantum chemical approach to a molecular framework. Atomic charges influenced dipole moment, polarizability, and molecular electronic structure. Ligand possessed four types of atoms (C, O, N, H) and showed a specific negative and positive value of Mulliken charges according to electronegativity of atoms. Oxygen and nitrogen atoms of ligand showed negative values, while all hydrogen atoms possessed positive values [33]. Moreover, it is noticed that the carbon atoms C1, C2, and C19 contain positive charges due to their direct attachment of electronegative oxygen atoms. Similarly, C5, C11, C12, and C17 also contain positive charges because of their direct attachment of electronegative nitrogen atoms. However, the carbon atoms C3, C4, C6, C18, C20, C21, C22, C24, and C32 have negative charges, because these carbon atoms do not have direct attachment with any electronegative atoms but bonded with relatively more electropositive hydrogen atoms [34, 35]; see Fig. 1 and Table S4.

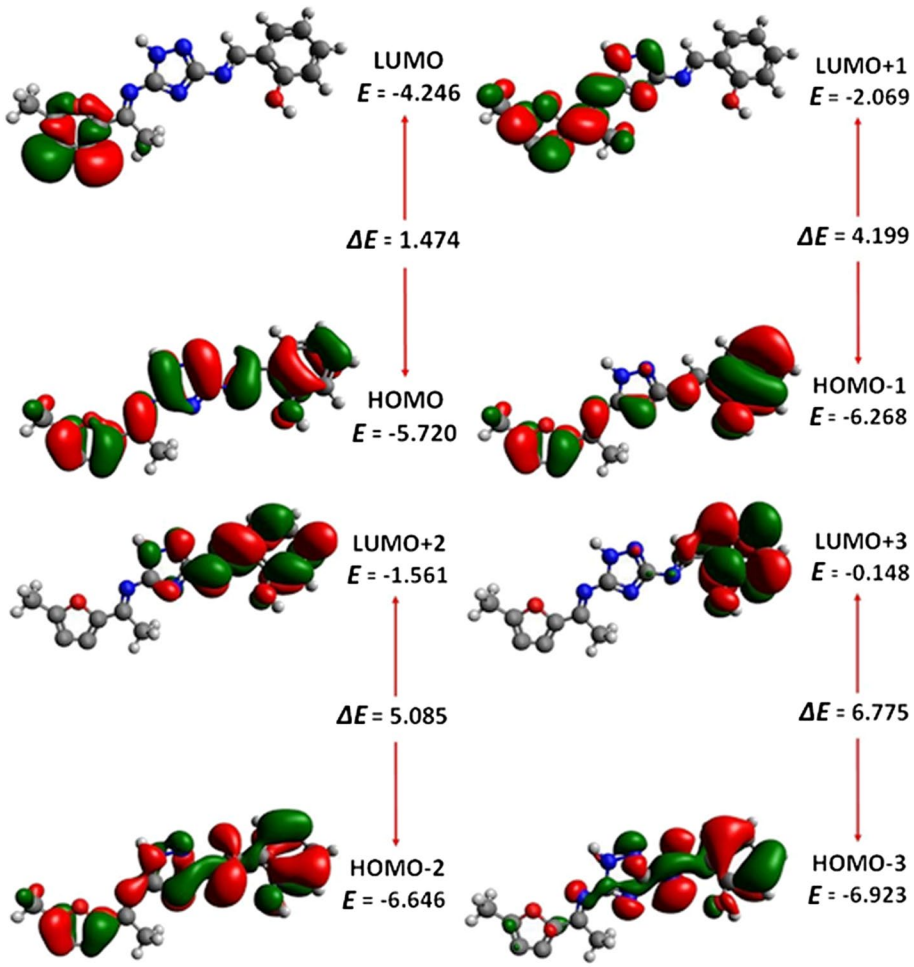

Fig. 2 The frontier molecular orbitals of ligand **L**, energies are reported in eV unit

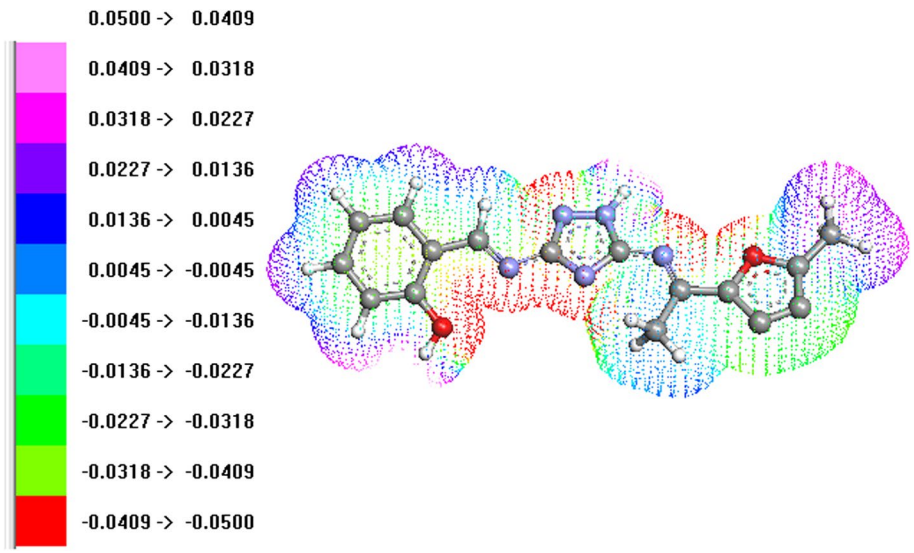

Fig. 3 Molecular electrostatic potential diagram of ligand **L**

IR spectral studies

The IR spectral studies strongly supported the formation of triazole ligand and spectral data are provided in Table S5. The appearance and disappearance of various types of peaks helped in understanding the structure of new synthesized triazole ligand. The azomethine (HC=N) band appeared at 1631 cm^{-1} which gave a clue that the condensation reaction

occurred between amino group of triazole and carbonyl group of 2-hydroxybenzaldehyde as well as 5-methyl-2-acetylfuran. The formation of ligand was also confirmed due to absence of other bands such as ν(C=O) functional group of 2-hydroxybenzaldehyde and 5-metyl-2-acetylfuran at 1715 and 1740 cm^{-1}, respectively. In IR spectra of ligand, the triazole moiety showed bands at 3456, 1611, and 1021 cm^{-1} due to vibration mode of ν(N–H), ν(C=N), and ν(N–N) bonds. The band appeared at 3137 cm^{-1} due to ν(OH) of 2-hydroxybenzaldehyde [36]. IR spectroscopy also provided information about coordination between ligand and metal ions. The IR value of azomethine linkage was reduced from 1629 to 1633 to 1617–1624 cm^{-1} in case of metal complexes as compared to IR spectra of ligand which indicated the formation of bonding between metal and triazole ligand. The IR value of ν(C=N) changed from 1611 to 1590–1597 cm^{-1} due to the coordination of nitrogen of triazole moiety with the metal. The coordination between metal and ligand was confirmed by the disappearance of OH band as well as by the appearance of a new peak ν(C–O) in the range of 1385–1390 cm^{-1}. In IR spectra of metal complexes of triazole, a new band appeared in the range of 516–524 cm^{-1} and the appearance of this vibration band provided evidence of presence of metal to nitrogen bond in metal complex. Appearance of another new band in IR spectra of metal complexes in a range of 421–427 cm^{-1} value gave a clue about metal to oxygen bonding [37]. Formation of vanadium complex was confirmed by the presence of new peak at 961 cm^{-1} due to the ν(V=O) vibration. All metal complexes showed no change in ν(N–H), ν(N–N), and ν(C=N) vibrations and provided information about their non-involvement in direct coordination between ligand and metal [38].

Measurements of magnetic moments and molar conductance

The magnetic moments of the synthesized metal complexes were calculated using Gouy balance and depicted in Table S5. This study helped in understanding the nature of ligand and coordination of metal complexes. Magnetic moment values help in predicting the diamagnetic and paramagnetic behavior of metal-based compounds. All the synthesized transitions of metal complexes possessed specific magnetic moment values due to presence of unpaired electrons in d-orbital. The vanadium metal complex showed 1.75 BM [39]. The chromium metal complex displayed magnetic moment value as 3.88 BM due to presence of three unpaired electrons in the d-orbital. The manganese and iron metal complexes showed 5.90 and 5.06 BM magnetic moment values leading to paramagnetic behavior of metal complexes [40]. The cobalt metal complex possessed 4.29 BM magnetic moment value, while copper metal complex possessed 1.81 BM magnetic moment values. The magnetic moment value of zinc metal complex was found to be zero. The zinc metal was found to be diamagnetic, while all other metal complexes were paramagnetic in nature [41].

The conductivities of the metal complexes were in the range of 10–20 Ω^{-1} cm^2 mol^{-1}. These values suggest the non-electrolytic nature of the complexes. The conductivity value of the chromium(III) metal complex was recorded 98 Ω^{-1} cm^2 mol^{-1}. The value indicated high conductivity of the complexes [42].

Bioactivity of synthesized compounds

Novel designed ligand and its metal-based compounds showed bactericidal action using four bacterial strains such as A = *Escherichia coli*, B = *Staphylococcus aureus*, C = *Neisseria gonorrhea*, and D = *Pseudomonas syringae* using agar diffusion method. The solutions were prepared in solvent (DMSO) as DMSO showed no activity against all selected bacterial strains. The activity results of all compounds were measured in zone of inhibition (mm) and compared with the standard drug kanamycin (Table S6, Fig. 4). The ligand and their metal complexes showed different results against different bacterial strains. The ligand showed 4–5 mm inhibitory growth against A–D bacterial strains and metal complexes displayed varying degree of inhibitory zone 5–10 mm against bacterial strains. Chromium and copper complexes showed highest inhibition of 10 mm against bacterial strain C and nickel complex demonstrated same inhibition of 10 mm against B. The metal complex **1** possessed highest 7–9 mm activity against A and D bacterial types as well as reported moderate 5–6 mm activity against C and B bacterium.

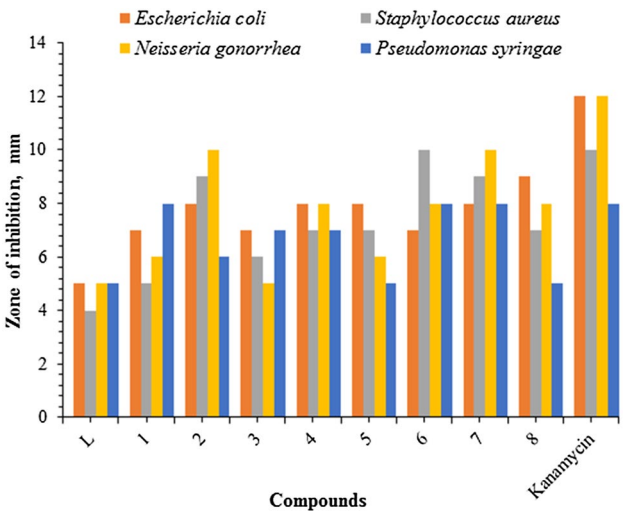

Fig. 4 Antibacterial activity of ligand **L** and metal complexes **1**–**8**

The compound **2** displayed highest as well as moderate zones of inhibitory such as 6–10 mm against A–D bacterial strains. The metal complexes **3**–**8** possessed 7–9 mm zone of inhibitory against A bacterial strain. The metal complexes such as **6**–**8** showed highest antibacterial activity against B as well as C bacterium types, while other compounds reported moderate antibacterial activity. The metal complexes **3** and **5**–**8** displayed good antibacterial results against D bacterial strain [43]. The variation in the activity of ligand and metal complexes against selected bacterial strains depend either on the impermeability of the cells of the microbes or difference in ribosomes of microbial cells. All the metal complexes exhibited good antibacterial results against selected bacterial strains than ligand due to chelation effect [44].

Conclusion

The unsymmetrical triazole ligand was prepared by the condensation reaction among triazole, 2-hydroxybenzaldehyde, and 5-methyl-2-acetylfuran. The ligand was obtained in good yield with specific color. The formation of ligand was confirmed by various methods such as color, solubility, melting point, and techniques like ^{1}H NMR, ^{13}C NMR, and MS. The synthesis of ligand was further supported by computational and frontier molecular orbital analysis. All the analyses revealed the synthesis, structure, nature, and electronic distribution of ligand. The synthesized ligand was used to prepare VO(IV), Cr(III), Mn(II), Fe(II), Co(II), Ni(II), Cu(II), and Zn(II) metal complexes. The prepared metal complexes were characterized by specific melting points, colors, IR, magnetic moments, and conductances. The metal ions coordinated with ligand using three sites of ligand. The magnetic moments of metal complexes helped in determining geometry of metal complexes. Antibacterial action of all the synthesized compounds was studied in vitro against *Escherichia coli*, *Staphylococcus aureus*, *Neisseria gonorrhea*, and *Pseudomonas syringae* bacterial strains. All the synthesized compounds exhibited good biological activity.

Experimental

The highly standard pure chemicals (Sigma-Aldrich and Merck) were used directly in the whole methodology. The solvents were indirectly utilized in all processes as distillation technique was used to purify solvents. The starting materials used in this work were 1,2,4-triazole-3,5-diamine, 2-hydroxybenzaldehyde, and 5-methyl-2-acetylfuran. Metallic salts $VOSO_4{\cdot}H_2O$, $CrCl_3{\cdot}6H_2O$, $MnCl_2{\cdot}2H_2O$, $FeSO_4{\cdot}7H_2O$, $CoCl_2{\cdot}6H_2O$, $NiCl_2{\cdot}6H_2O$, $CuCl_2{\cdot}2H_2O$, and $ZnCl_2{\cdot}2H_2O$ were used for the synthesis of metal complexes with purity. Melting points of all the compounds were determined by Stuart melting point apparatus in open glass capillaries and were recorded. Distilled ethanol was used as solvent for the synthesis ligand and their metal complexes. TLC (silica gel-G plates) was utilized to monitor the synthesis of obtained compounds. Spectrophotometer as Hitachi UV-3200 was used to record UV Spectra. JEOL MS Route instrument was used to record mass spectrum of ligand. Infrared spectrometer (Nicolet FT-IR Impact 400 D) was utilized to record IR spectra of the newly formed ligand as well as metal-based compounds using matrix of KBr in the range 3700–370 cm^{-1}. Magnetic susceptibilities of the complexes were measured at room temperature by the Gouy method at room temperature using a model Stanton SM12/S Gouy balance. The ^{1}H NMR and ^{13}C NMR spectra were recorded with Bruker Avance 300 MHz instrument, using DMSO-d_6 as solvent. The conductometric measurements of the metal-based compounds were performed in DMSO solvent with Inolab Cond 720 Conductivity meter on room temperature. Antibacterial studies were taken out in Biochemistry and Biotechnology Research Lab, University of Gujrat, Pakistan.

2-[[[5-[[1-(5-Methylfuran-2-yl)ethylidene]-amino]-1*H*-1,2,4-triazol-3-yl]imino]methyl]phenol (L, $C_{16}H_{15}N_5O_2$) The compound 1,2,4-triazole-3,5-diamine (5 mmol) first formed a solution with ethanol solvent, then was magnetically refluxed with 5-methyl-2-acetyl furan (5 mmol) for 8 h in a 100 cm^3 round-bottom flask. A light color change was observed and then added 2-hydroxybenzaldehyde (5 mmol) and refluxed for 4 h. A yellow precipitate was formed which gave the first indication of formation of ligand. The whole reaction was observed by TLC method. Precipitates of ligand were washed with ethanol and also cooled, filtered as well as dried at room temperature. Yield: 2.45 g (75%); yellow solid; m.p.: 236 °C; ^{1}H NMR (DMSO-d_6): $\delta = 2.49$ (s, CH_3), 3.32 (s, CH_3), 6.95 (s, 1H), 7.00 (s, 1H), 7.40 (t, 1H), 7.49 (t, 1H), 7.67 (d, 1H), 7.85 (d, 1H), 12.79 (s, OH), 14.28 (s, N=CH) ppm; ^{13}C NMR (DMSO-d_6): $\delta = 13.56$ (C16), 13.70 (C11), 116.55 (C2), 119.08 (C6), 119.27 (C4), 132.44 (C5), 133.39 (C3), 156.68 (C6), 160.19 (C6), 161.68 (C7), 163.07 (C10) ppm; IR (KBr): $\overline{\nu} = 3137$ (OH), 3456 (NH), 1631 (HC=N), 1611 (triazole, C=N), 1391 (C–O), 1021 (N–N) cm^{-1}; MS (EI, 70 eV): *m/z* (%) = 308.1 ([M]$^+$, 12), 290 (100), 203 (23.6), 147.1 (20), 132 (10), 77 (21.3), 43 (19).

Synthesis of transition metal-based compounds 1–8

Metal-based compounds of ligand were synthesized by adding 10 mmol of ligand and 1 cm^3 ethanol solution of 5 mmol of metal salt in 10 cm^3 distilled ethanol. During refluxing,

the precipitates were formed and solid product was collected after filtration. The precipitates of metal complexes were dried at room temperature. When metal complexes were dried and weighed, yield was calculated. The whole reactions were monitored by TLC. All complexes were recrystallized in an equimolar solution of ethanol and methanol. All the metal complexes were prepared in 1:2 (M:L) molar ratio. Metal complexes of ligand possessed characteristic color and melting points.

Bis-2-[[[5-[[1-(5-Methylfuran-2-yl)ethylidene]-amino]-1*H*-1,2,4-triazol-3-yl]imino]methyl]phenolido-oxovanadium(IV) (1, $C_{32}H_{28}N_{10}O_5V$) Yield: 2.65 g (77%); color: green; m.p.: 274–275 °C; IR (KBr): $\overline{\nu}=1621$ (HC=N), 1387 (C–O), 961 (V=O), 424 (V–O), 518 (V–N) cm^{-1}; conductance: $\Omega_M=15\ \Omega^{-1}\ cm^2\ mol^{-1}$; magnetic moment: $\mu_{eff}=1.75$ BM.

Bis-2-[[[5-[[1-(5-Methylfuran-2-yl)ethylidene]-amino]-1*H*-1,2,4-triazol-3-yl]imino]methyl]phenolido-chromium(III) chloride (2, $C_{32}H_{28}ClCrN_{10}O_4$) Yield: 2.50 g (71%); color: dark green; m.p.: 137–138 °C; IR (KBr): $\overline{\nu}=1617$ (HC=N), 1388 (C–O), 521 (Cr–N), 426 (Cr–O) cm^{-1}; conductance: $\Omega_M=98.1\ \Omega^{-1}\ cm^2\ mol^{-1}$; magnetic moment: $\mu_{eff}=3.88$ BM.

Bis-2-[[[5-[[1-(5-Methylfuran-2-yl)ethylidene]-amino]-1*H*-1,2,4-triazol-3-yl]imino]methyl]phenolido-manganese(II) (3, $C_{32}H_{28}MnN_{10}O_4$) Yield: 2.89 g (80%); color: pink; m.p.: 269–271 °C; IR (KBr): $\overline{\nu}=1622$ (HC=N), 1385 (C–O), 520 (Mn–N), 421 (Mn–O) cm^{-1}; conductance: $\Omega_M=11\ \Omega^{-1}\ cm^2\ mol^{-1}$; magnetic moment: $\mu_{eff}=5.90$ BM.

Bis-2-[[[5-[[1-(5-Methylfuran-2-yl)ethylidene]-amino]-1*H*-1,2,4-triazol-3-yl]imino]methyl]phenolido-iron(II) (4, $C_{32}H_{28}FeN_{10}O_4$) Yield: 2.55 g (76%); color: light green; m.p.: 251–253 °C; IR (KBr): $\overline{\nu}=1618$ (HC=N), 1391 (C–O), 523 (Fe–N), 427 (Fe–O) cm^{-1}; conductance: $\Omega_M=17\ \Omega^{-1}\ cm^2\ mol^{-1}$; magnetic moment: $\mu_{eff}=5.06$ BM.

Bis-2-[[[5-[[1-(5-Methylfuran-2-yl)ethylidene]-amino]-1*H*-1,2,4-triazol-3-yl]imino]methyl]phenolido-cobalt(II) (5, $C_{32}H_{28}CoN_{10}O_4$) Yield: 2.51 g (74%); color: brown; m.p.: 228–229 °C; IR (KBr): $\overline{\nu}=1619$ (HC=N), 1390 (C–O), 519 (Co–N), 423 (Co–O) cm^{-1}; conductance: $\Omega_M=16\ \Omega^{-1}\ cm^2\ mol^{-1}$; magnetic moment: $\mu_{eff}=4.29$ BM.

Bis-2-[[[5-[[1-(5-Methylfuran-2-yl)ethylidene]-amino]-1*H*-1,2,4-triazol-3-yl]imino]methyl]phenolido-nickel(II) (6, $C_{32}H_{28}N_{10}NiO_4$) Yield: 2.66 g (79%); color: parrot green; m.p.: 126–128 °C; IR (KBr): $\overline{\nu}=1624$ (HC=N), 1387 (C–O), 517 (Ni–N), 426 (Ni–O) cm^{-1}; conductance: $\Omega_M=14\ \Omega^{-1}\ cm^2\ mol^{-1}$; magnetic moment: $\mu_{eff}=2.97$ BM.

Bis-2-[[[5-[[1-(5-Methylfuran-2-yl)ethylidene]-amino]-1*H*-1,2,4-triazol-3-yl]imino]methyl]phenolido-copper(II) (7, $C_{32}H_{28}CuN_{10}O_4$) Yield: 2.57 g (76%); color: dark green; m.p.: 195–196 °C; IR (KBr): $\overline{\nu}=1620$ (HC=N), 1389 (C–O), 524 (Cu–N), 425 (Cu–O) cm^{-1}; conductance: $\Omega_M=12\ \Omega^{-1}\ cm^2\ mol^{-1}$; magnetic moment: $\mu_{eff}=1.81$ BM.

Bis-2-[[[5-[[1-(5-Methylfuran-2-yl)ethylidene]-amino]-1*H*-1,2,4-triazol-3-yl]imino]methyl]phenolido-zinc(II) (8, $C_{32}H_{28}N_{10}O_4Zn$) Yield: 2.83 g (83%); color: off white; m.p.: 216–217 °C; IR (KBr): $\overline{\nu}=1623$ (HC=N), 1386 (C–O), 516 (Zn–N), 427 (Zn–O) cm^{-1}; conductance: $\Omega_M=19\ \Omega^{-1}\ cm^2\ mol^{-1}$; magnetic moment: $\mu_{eff}=0$ BM.

Computational analysis

All density functional theory (DFT)-based calculations were carried out using Gaussian 09 software package [45]. Literature survey demonstrated that Minnesota density functionals especially M06-2X are a more accurate method for explaining the non-covalent interactions (NCIs), vibrational frequencies, bond lengths, and excitation energies in comparison with other functionals [46]. Therefore, the geometric parameters and frequency calculations of the ligand were performed by M06-2X/6-311G (d, p) and negative frequency could be not found in said calculations. The absence of negative eigenvalues showed that the optimized ligand was found at true minima on the potential energy surface. FMOs, NPA, and MEP were analyzed by utilizing M06-2X/6-311G (d, p) method. UV–Vis analysis has been executed with TD-DFT/M06-2X/6-311G (d, p). Chemcraft was used for the preparation of input and analysis.

Biological activities

Anti-bacterial activities of triazole ligand as well as transition metal-based compounds were tested against selected Gram-positive and Gram-negative bacterial strains by disc diffusion. First gel was formed for the antibacterial activities from an equal amount of agar agar and nutrient broth. Agar agar and nutrient broth were heated up to boiling in distilled water. Petri dishes and the above solution were autoclaved for 20 min. A mixture of gel as well as bacterial species was placed into petri dishes. The compounds were placed on paper discs. Petri dishes were completely covered and placed into an incubator for 30 h. Finally, the zone of inhibition was measured [47, 48].

Acknowledgements The authors are thankful to the Higher Education Commission (HEC) of Pakistan for providing financial support through the NRPU Project # 7800.

References

1. Chohan ZH, Hanif M (2013) J Enz Inhib Med Chem 28:944
2. Maertens JA (2004) Clin Microbiol Infect 10:1
3. Dismukes WE (2000) Clin Infect Dis 30:653
4. Zonios DI, Bennett JE (2008) Semin Respir Crit Care Med 29:198
5. Gupta AK, Tomas E (2003) Dermatol Clin 21:565
6. Vashi K, Naik HB (2004) Eur J Chem 1:272
7. Ferreira M, Pinheiro L, Santos-Filho O, Peçanha M, Sacramento C, Machado V, Ferreira V, Souza T, Boechat N (2014) Med Chem Res 23:1501
8. Desai KG, Desai KR (2006) J Heterocycl Chem 43:1083
9. Sun X, Bai Y, Liu Y, Chen B (2010) Acta Chim Sin 68:788
10. Sachdeva H, Dwivedi D, Arya K, Khaturia S, Saroj R (2013) Med Chem Res 22:4953
11. Küçükgüzel I, Güniz KS, Rollas S, Ötük-Saniş G, Özdemir O, Bayrak I, Altuğ T, Stables JP (2004) Farmaco 59:893
12. Basavapatna N, Kumar P, Kikkeri NM, Lingappa M (2013) J Fluor Chem 156:15
13. Sondhi SM, Arya S, Rani R, Kumar N, Roy P (2012) Med Chem Res 21:3620
14. Singh R, Chouhan A (2014) World J Pharm Pharma 3:874
15. Bekircan O, Menteşe E, Ülker S (2014) Arch Pharm Chem Life Sci 347:387
16. Ehsan S, Sarfraz S, Khan B, Hassan SM, Iqbal M (2016) Chem Int 2:262
17. Yusuf M, Jain P (2011) Arabian J Chem 7:604
18. Udupi RH, Manjunath CJ (2018) J Pharm Sci Res 10:420
19. Korcz M, Franciszek SA, Patrick JB, Anita K (2018) Molecules 23:1497
20. Hany M, Dalloul HM, El-nwairy K, Shorafa AZ, Samaha AA (2017) Org Commun 10:280
21. Goel P, Kumar D, Chandra SJ (2014) Chem Bio Phy Sci Sec 4:1946
22. Mobinikhaledi A, Forughifar N, Kahlor M (2010) Turk J Chem 34:36
23. Zhang R, Wang Q, Li Q, Ma C (2009) Inorg Chim Acta 362:2762
24. Xie XF, Chen SP, Xia ZQ, Gao SL (2009) Polyhedron 28:679
25. Sumrra SH, Chohan ZH (2010) Appl Organomet Chem 24:122
26. Chohan ZH, Hanif M (2010) J Enz Inhib Med Chem 25:737
27. Temel H, Çakir U, Otludil B, Uğraş HI (2001) Synth React Inorg Met Org Chem 31:1323
28. Akram M, Adeel M, Khalid M, Tahir MN, Khan MU, Asghar MA, Ullah MA, Iqbal M (2018) J Mol Struct 1160:129
29. Ahmad MS, Khalid M, Shaheen MA, Tahir MN, Khan MU, Braga AAC, Shad HA (2017) J Phys Chem Solids 115:265
30. Koopmans TA (1993) Physica 1:104
31. Lesar A, Milosev I (2009) Chem Phys Lett 483:198
32. Alphonsa AT, Loganathan C, Anand SAA, Kabilan S (2016) J Mol Struct 1106:277
33. Dheivamalar S, Sugi L, Ambigai K (2016) Comput Chem 4:17
34. Rajaraman D, Sundararajan G, Rajkumar R, Bharanidharan S, Krishnasamy K (2016) J Mol Struct 1108:698
35. Reem I, Al-Wabli, Manimaran D, John L, Joe IS, Haress NG, Attia MI (2016) J Spectrosc 2016:1
36. Yaul A, Pethe G, Deshmukh R, Aswar A (2013) J Therm Anal Calorim 113:745
37. Chohan ZH, Sumrra SH, Youssoufi MH, Hadda TB (2010) Eur J Med Chem 45:2739
38. Pranita U, Gawande PR, Mandlik S, Swar A (2015) Indian J Pharm Sci 77:376
39. Srivastava AN, Singh NP, Shriwastaw CK (2014) J Serb Chem Soc 79:421
40. Maihub AA, Alassbaly FS, El-Ajaily MM, Etorki AM (2014) Green Sustain Chem 4:103
41. Chen KY, Tsai HY (2014) Int J Mol Sci 15:18076
42. Yu Y, Chen S, Li X, Jin S, Li L, Zhang G, Mab X, Shu Q (2017) RSC Adv 71:8523
43. Sumrra SH, Ramzan S, Mustafa G, Ibrahim M, Mughal EU, Nadeem MA, Chohan ZH, Khalid M (2018) Russ J Gen Chem 88:1707
44. Sumrra SH, Kausar S, Raza MA, Zubair M, Zafar MN, Nadeem MA, Mughal EU, Chohan ZH, Mushtaq F, Rashid U (2018) J Mol Struct 1168:202
45. Arjunan V, Sakiladevi S, Rani T, Mythili C, Mohan S (2012) Spectrochim Acta A 88:220
46. Mardirossian N, Head-Gordon M (2016) J Chem Theory Comput 12:4303
47. Sumrra SH, Atif AH, Zafar MN, Khalid M, Tahir MN, Nazar MF, Nadeem MA, Braga AAC (2018) J Mol Struct 1166:110
48. Sumrra SH, Mushtaq F, Khalid M, Raza MA, Nazar MF, Ali B, Braga AAC (2018) Spectrochim Acta A 190:197

Affiliations

Sajjad H. Sumrra[1] · Ifza Sahrish[1] · Muhammad A. Raza[1] · Zahoor Ahmad[3] · Muhammad N. Zafar[2] · Zahid H. Chohan[4] · Muhammad Khalid[5] · Saeed Ahmed[5]

✉ Sajjad H. Sumrra
sajjadchemist@uog.edu.pk

✉ Muhammad Khalid
muhammad.khalid@kfueit.edu.pk

[1] Department of Chemistry, University of Gujrat, Gujrat 50700, Pakistan

[2] Department of Chemistry, Quaid-I-Azam University, Islamabad 45320, Pakistan

[3] Department of Chemistry, University of Engineering and Technology, Lahore, Pakistan

[4] Department of Chemistry, University College of Management and Sciences, Khanewal, Pakistan

[5] Department of Chemistry, Khwaja Fareed University of Engineering and Information Technology, Rahim Yar Khan 64200, Pakistan